# Equatorial Kelvin wave signatures in ozone profile measurements from Global Ozone Monitoring Experiment (GOME)

R. M. A. Timmermans[1] and R. F. van Oss
Royal Netherlands Meteorological Institute, De Bilt, Netherlands

H. M. Kelder
Royal Netherlands Meteorological Institute, De Bilt, Netherlands

Department of Applied Physics, Eindhoven University of Technology, Eindhoven, Netherlands

[1] This study investigates the ability to derive height-resolved information on equatorial Kelvin wave activity from three different Global Ozone Monitoring Experiment (GOME) ozone profile data sets. The ozone profiles derived using the Ozone Profile Retrieval Algorithm (OPERA) based on optimal estimation and the Neural Network Ozone Retrieval System (NNORSY) both show Kelvin wave signals in agreement with previously identified signals in the GOME total ozone columns. However, because of the inadequate vertical resolution, these two data sets are not able to resolve the vertical structure of the Kelvin wave activity. The third data set, consisting of assimilated OPERA ozone profiles, does provide height-resolved information on Kelvin wave activity that is consistent with results from the analysis of GOME total ozone columns and ECMWF Re-Analysis (ERA-40) temperature data. Largest Kelvin-wave-induced perturbations of up to 0.69 DU/km coincide with the maximum vertical gradient in ozone around 35 hPa and show an in-phase relationship with temperature perturbations in ERA-40 as expected from theoretical considerations. These results indicate that the ozone perturbations in the lower stratosphere and in the total column of ozone are transport related. Between 10 and 1 hPa, large Kelvin-wave-induced fluctuations in ozone mixing ratio are present that, however, because of their small contribution to the total column, do not constitute a large contribution to the total ozone column perturbations. The ozone perturbations between 10 and 1 hPa show an out-of-phase relationship with temperature perturbations in ERA-40, indicating that the perturbations can either be caused by transport effects or photochemical influences.

Citation: Timmermans, R. M. A., R. F. van Oss, and H. M. Kelder (2005), Equatorial Kelvin wave signatures in ozone profile measurements from Global Ozone Monitoring Experiment (GOME), *J. Geophys. Res.*, *110*, D21103, doi:10.1029/2005JD005929.

## 1. Introduction

[2] The equatorial Kelvin wave is one of the important types of waves present in the tropics. It is an eastward and vertically propagating wave. Because of its vertical propagation it can transport eastward momentum upward and thereby play a role in the driving of the quasi-biennial and semiannual oscillations in the zonal wind [e.g., *Andrews et al.*, 1987]. In spite of their importance in the atmosphere, the climatology of equatorial Kelvin waves is still not very well known. Kelvin wave signatures have been detected in data sets from ground-based instruments [e.g., *Wallace and Kousky*, 1968; *Hirota*, 1978; *Boehm and Verlinde*, 2000; *Holton et al.*, 2001]. A drawback of using ground-based measurements to investigate Kelvin waves is the lack of regularly operating stations around the equator, giving a poor horizontal coverage. Satellite measurements provide a mean to study the global distribution of Kelvin wave activity. Different satellite instruments have been used to study Kelvin wave signatures in either temperature or trace gas measurements [see, e.g., *Salby et al.*, 1990; *Randel and Gille*, 1991; *Ziemke and Stanford*, 1994; *Canziani*, 1999; *Smith et al.*, 2002; *Kawamoto et al.*, 1997; *Mote and Dunkerton*, 2004] (see *Timmermans et al.* [2005] for a more complete overview of previous satellite-borne observations on Kelvin waves). The studies that treat ozone Kelvin waves [e.g., *Kawamoto et al.*, 1997; *Mote and Dunkerton*, 2004] show dominant ozone mixing ratio variations at the level where the vertical gradient in zonal mean ozone is

---

[1]Now at Environment, Health, and Safety, Netherlands Organisation for Applied Scientific Research TNO, Apeldoorn, Netherlands.

largest. These variations are attributed to dynamical advection of ozone and are in phase with temperature variations. A second maximum in ozone variability due to Kelvin waves is often found in the upper stratosphere, attributable to photochemical perturbations. These variations show an out-of-phase relationship with temperature variations.

[3] In previous studies, *Timmermans et al.* [2004, 2005] (hereinafter referred to as T04 and T05) demonstrated the sensitivity of the Global Ozone Monitoring Experiment (GOME) ozone column measurements to Kelvin waves. In seven years of data, three periods of high Kelvin wave activity were found correlating with Kelvin wave signatures in European Centre for Medium-Range Weather Forecasts (ECMWF) Re-Analysis (ERA-40) data. The ERA-40 zonal wind and temperature data provide information on the vertical structure of the Kelvin wave activity found in the GOME total ozone columns.

[4] To study the vertical distribution of the ozone fluctuations induced by Kelvin waves, ozone profile measurements are needed. In this study we investigate the vertical structure of the previously identified Kelvin waves by using ozone profiles measured by GOME. For this we will investigate three different data sets derived from the GOME measurements. The first consists of ozone profiles retrieved using the Ozone Profile Retrieval Algorithm (OPERA) based on optimal estimation [*van der A et al.*, 2002; *van Oss and Spurr*, 2002]. The second data set consists of ozone profiles derived using the Neural Network Ozone Retrieval System (NNORSY) [*Müller et al.*, 2003]. The third data set consists of assimilated ozone profiles based on the above mentioned OPERA ozone profiles which are assimilated using the TM3 model driven by the ECMWF (ERA-40) meteorology [*Segers et al.*, 2004]. It must be noted that this third data set is not an independent data set and the results are dependent on the signatures in the ERA-40 data set. However, the assimilated data set forms an optimal combination between the ozone profile measurements and the information from the ERA-40 data to provide the best representation of the ozone distribution. This representation can be used to study the vertical distribution of the ozone fluctuations induced by the Kelvin waves previously identified in T04 and T05. The three data sets all have different characteristics concerning for instance accuracy and vertical resolution and will therefore give different results. The following section provides some details on the three data sets.

## 2. Data and Analysis
### 2.1. GOME Instrument

[5] The GOME instrument was launched on 21 April 1995 on board the European Remote Sensing Satellite (ERS-2). It is a nadir-viewing spectrometer that measures the radiation of the Sun that is scattered by the Earth's atmosphere or reflected from the Earth's surface. The measured radiation provides information on the ozone concentration in the atmosphere [*Burrows et al.*, 1999]. The amount of absorbed radiation by ozone is dependent on the wavelength of the radiation; that is, radiation with a wavelength of 265 nm is more strongly absorbed than radiation with a wavelength of 350 nm. Because of this, the 265 nm radiation from the Sun will not reach the lower part of the atmosphere and only contain information on the upper layers of the atmosphere, while the 350 nm radiation will be able to pass through the entire atmosphere and contain information on the total ozone column. When going from 265 to 350 nm, the radiation will gradually reach deeper in the atmosphere and contain information on a larger vertical part of the atmosphere. The wavelength dependence of ozone absorption thus allows the derivation of information on the vertical distribution of ozone. The spatial resolution of the GOME ozone profile measurements is 100 km in latitudinal and 960 km in longitudinal direction. Global coverage is reached in three days.

### 2.2. OPERA O$_3$ Profiles

[6] The OPERA algorithm, used to derive the ozone profiles in this data set, is based on the optimal estimation method, where information of the observation is combined with a priori information. To get the best estimate, the difference between observations and predictions from a forward model as well as the difference between the a priori information and the estimated parameters are minimized. The balance of these both contributions is determined using the observational errors and the errors in the a priori values. The Linearized Discrete Ordinate Radiative Transfer (LIDORT) radiative transfer model is used to calculate the expected reflectance measured by the instrument, given a prescribed atmospheric composition. A priori profiles are taken from an ozone climatology by *Fortuin and Kelder* [1998]. This is a zonal mean ozone climatology based on a 12 year observation period of ozone sonde stations and satellites. Because of the inclusion of an a priori profile, the retrieved profiles is a mixture between true and the a priori profile. The relation between retrieved profile x$_{retrieved}$, true profile x$_{true}$ and a priori profile x$_{apriori}$ is given by

$$x_{retrieved} - x_{apriori} = A(x_{true} - x_{apriori}) + \epsilon \qquad (1)$$

$\epsilon$ is the random or retrieval error which results from random errors in the GOME radiance measurements. Its magnitude varies between a few percent in the lower and middle atmosphere, rising to 10% in the troposphere and higher stratosphere. The averaging kernel A is a measure for the limited ability of the retrieval to find the true profile. It relates the true anomaly (truth minus a priori profile) to the retrieved anomaly (retrieval minus a priori). The limited profile information in the spectral measurement appears in the averaging kernel as broad weighting functions indicating that the retrieved value at some altitude depends on the true profile in a certain vertical range around that altitude. The vertical extent of the averaging kernel can be viewed as the vertical resolution. A second feature of the averaging kernel is that it shows small values in regions for which there is little profile information in the measurement. This leads to a small retrieved anomaly in this region, or a retrieved value close to the a priori. In other words, the optimal estimation retrieval tends to the a priori in case the measurement contains little information.

[7] For a more detailed description of the algorithm we refer the reader to *van der A et al.* [2002] and *van Oss and Spurr* [2002]. For more information on the vertical resolution and the quality of the profiles we refer the reader to *Meijer et al.* [2003].

[8] From equation (1) it can be concluded that temporal and spatial variations in the retrieved profile are not influenced by the a priori since a constant a priori profile is used for the spatial and temporal range considered. Only the random error affects the results of the variability analysis. Note that this random error is considerably decreased by the averaging of the profiles before the analysis as described in section 2.5.

[9] Spatial variations in the vertical direction are influenced by the averaging kernel; however, waves with a vertical wavelength smaller or comparable to the width of the averaging kernel in the true profile are damped in the retrieved profile. This has indeed been found in the results described in section 3.3.

[10] The ozone profiles used in this study consist of ozone column densities for 40 vertical layers which are defined by 41 pressure levels between the surface and 0.1 hPa. The vertical resolution that can be resolved is about 5 km around the ozone maximum and poorer at other altitudes. The best accuracy is reached between 15 and 40 km. Outside this altitude range the accuracy rapidly decreases; therefore the focus of this study will lie within the altitude range of 15−40 km.

## 2.3. NNORSY O₃ Profiles

[11] Another approach to derive ozone profile information from GOME data is the use of neural networks, as is done with the Neural Network Ozone Retrieval system, NNORSY [*Müller et al.*, 2003]. This approach assumes a mapping between the spectral data measured by GOME and the ozone profile, which can be approximated by a neural network R according to

$$x = R(y, c, w) + \epsilon \qquad (2)$$

where x is the ozone profile, y is the spectrum measured by GOME, c is a vector with supplementary input data, w contains the network model parameters, also called weights, and $\epsilon$ is an error vector.

[12] To find an optimal set of weights, the system has to be trained using a training data set which consists of paired GOME spectral measurements and colocated ozone profile measurements from sondes and satellites. Once this is done, the neural network R can be applied to all observations.

[13] Apart from spectral data, the network is fed with some geophysical parameters which include satellite and solar zenith angles, scan angle, pixel type (east, west or nadir), latitude and season, in-orbit time and a temperature profile from the UK Meteorological Office (UKMO).

[14] The NNORSY ozone profiles are estimated to have a vertical resolution of at best 3−5 km at geopotential heights of 15−32 km.

[15] Comparisons of the NNORSY profiles with colocated ground based profile measurements that have not been used in the training, show that the accuracy of the ozone profiles is slightly better than the optimal estimation ozone profiles, most notably in the troposphere. There is no explicit relation between the true and retrieved profiles as for the optimal estimation retrieval, so random errors cannot be easily distinguished from other errors. The NNORSY profiles are, however, also affected by a smoothing error quantified by the vertical resolution of 4−6 km. This vertical smoothing will affect the analysis of spatial variation as for the optimal estimation profiles.

[16] For more details on this neural network approach we refer the reader to *Müller et al.* [2003].

## 2.4. Assimilated OPERA O₃ Profiles

[17] Retrieved ozone profiles from GOME, which are described in section 2.2, are being assimilated in the three-dimensional global chemistry-transport model TM3. One of the purposes is to get a better simulation of the vertical ozone distribution [*Segers et al.*, 2004]. The transport model has been configured to simulate the global concentration of ozone on 44 levels up to 0.1 hPa. The horizontal resolution is 3° in longitude and 2° in latitude. The ozone chemistry is parameterized using a simple homogeneous chemistry (Cariolle scheme [*Cariolle and Déqué*, 1986; *McLinden et al.*, 2000]) and heterogeneous chemistry based on chlorine activation [*Hadjinicolaou and Pyle*, 2004]. The model is driven by the meteorological fields from the ECMWF.

[18] The assimilation scheme is an extension of an existent assimilation scheme for total ozone columns. The scheme makes use of a three-dimensional covariance model that accounts for the different correlation scales in ozone with respect to altitude and longitude. It also makes use of the averaging kernel information supplied with the O₃ profiles.

[19] Comparisons with colocated ozone sonde measurements showed an accuracy of 5−20%, except for the tropical troposphere and the polar winter were the errors appeared to be larger [*Segers et al.*, 2004]. The variability analysis is only affected by random errors, except in the vertical direction where, again, the limited resolution will smooth the waves. However, it can be expected that the model "fills in" the vertical structures caused by transport since the meteorological input data is given on a densely sampled grid. From the comparison with ozone sondes in Figure 9 of *Segers et al.* [2004] it can be tentatively concluded that the vertical resolution of the assimilated profiles is a few kilometers, so much smaller than the retrieved profiles.

[20] For a more detailed description of the assimilation of GOME O₃ profiles, we refer the reader to *Segers et al.* [2004].

## 2.5. Analysis Method

[21] For the detection of Kelvin wave signals in the ozone profiles, the same bidimensional spectral analysis method as applied in T04 and T05 has been used. The method has the advantages to be able to handle unequally spaced data and to allow easy determination of the significance of detected signals. It is an extended version of the one-dimensional Lomb periodogram [*Press et al.*, 1992; *Scargle*, 1982], which allows the application to two-dimensional data sets. Here we will apply the periodogram to each level separately, i.e., data as function of longitude and time.

[22] Considering variable $h(t_j, x_l)$ measured at times $t_j$ with j = 1, 2,..., $N_t$ and locations $x_l$ with l = 1, 2,..., $N_x$, the extended Lomb normalized periodogram as function of angular frequency $\omega$ and zonal wave number $k$ is given by

$$P_N(\omega, k) \equiv \frac{1}{2\sigma^2} \left[ \frac{\left[ \sum_{j,l} \left( h_{j,l} - \bar{h} \right) \cos\left( \omega(t_j - \tau_1) \pm k(x_l - \tau_2) \right) \right]^2}{\sum_{j,l} \cos^2\left( \omega(t_j - \tau_1) \pm k(x_l - \tau_2) \right)} \right. $$
$$\left. + \frac{\left[ \sum_{j,l} \left( h_{j,l} - \bar{h} \right) \sin\left( \omega(t_j - \tau_1) \pm k(x_l - \tau_2) \right) \right]^2}{\sum_{j,l} \sin^2\left( \omega(t_j - \tau_1) \pm k(x_l - \tau_2) \right)} \right]$$

$$(3)$$
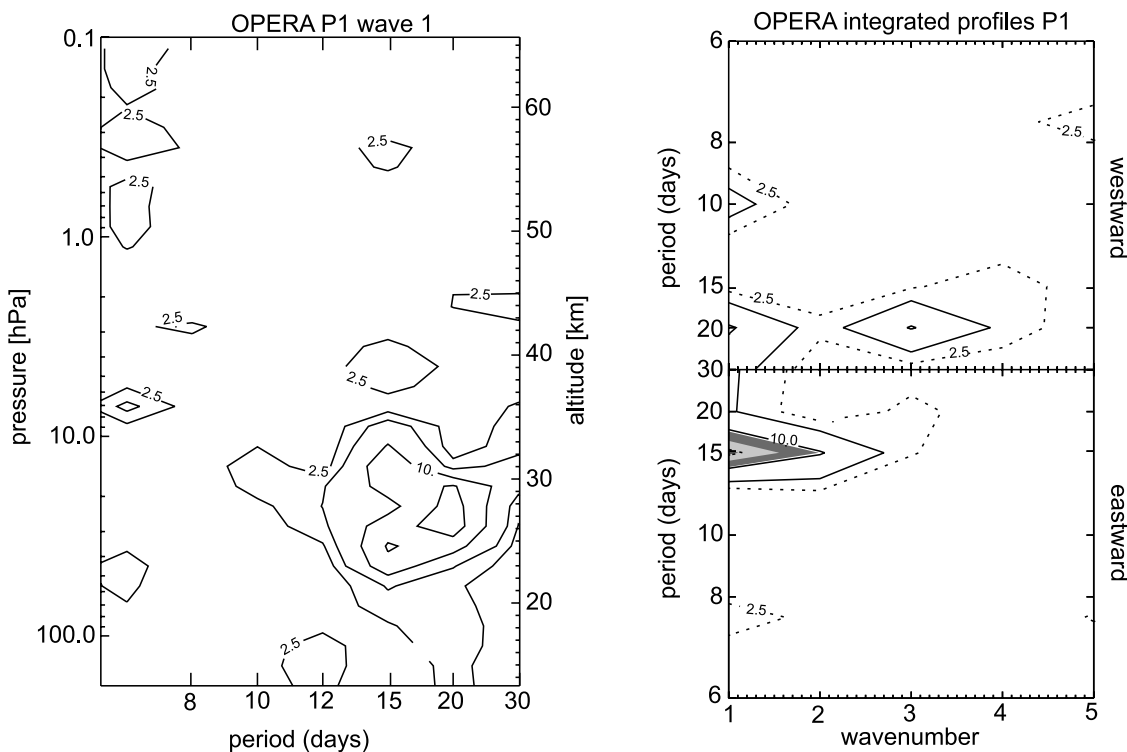
**Figure 1.** (left) Lomb periodogram for the OPERA ozone profiles, for zonal wave number 1 for the period 15 July to 13 September 1996. (right) Lomb periodogram for integrated OPERA ozone profiles for the period 15 July to 13 September 1996. See color version of this figure at back of this issue.
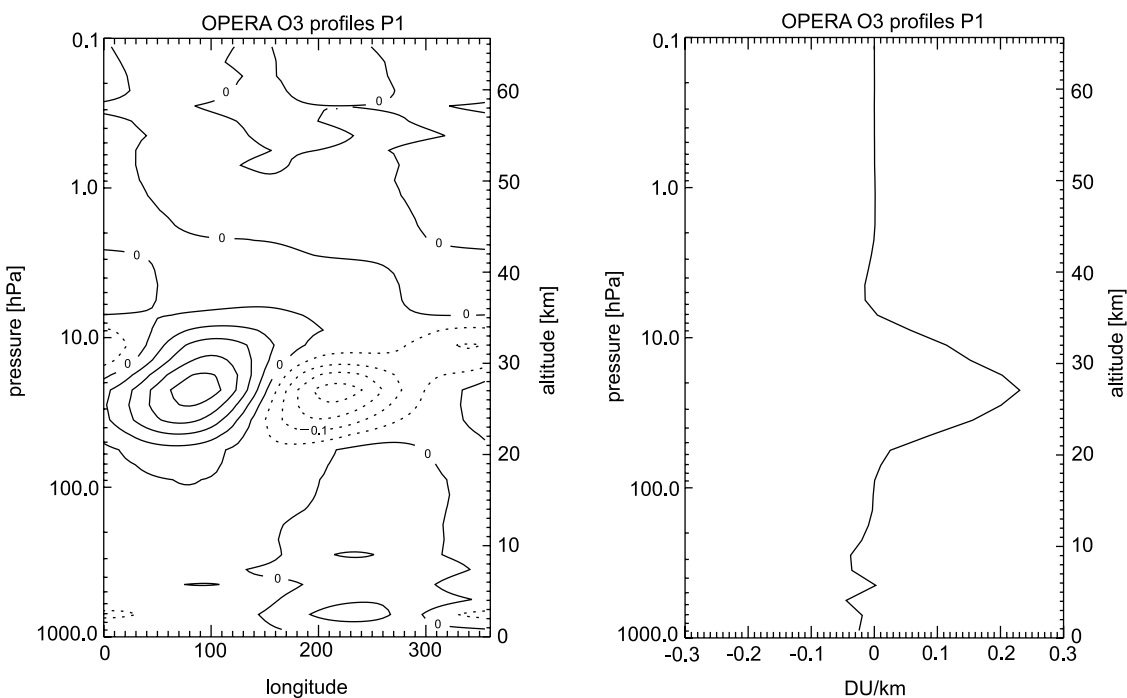


**Figure 2.** (left) Pressure versus longitude plot of waves 1 and 2 in the OPERA ozone profiles on 23 August 1996. A band-pass filter with half-amplitudes at 12 and 20 days has been applied. Solid lines start at 0 DU/km with increments of 0.05 DU/km for each contour line. Dashed lines start at −0.05 DU/km with a decrement of 0.05 DU/km for each contour line. Here, 1 DU = 2.687 × 10¹⁶ molecules/cm². (right) Profile of the ozone perturbations on 23 August 1996 at longitude equal to 85°.
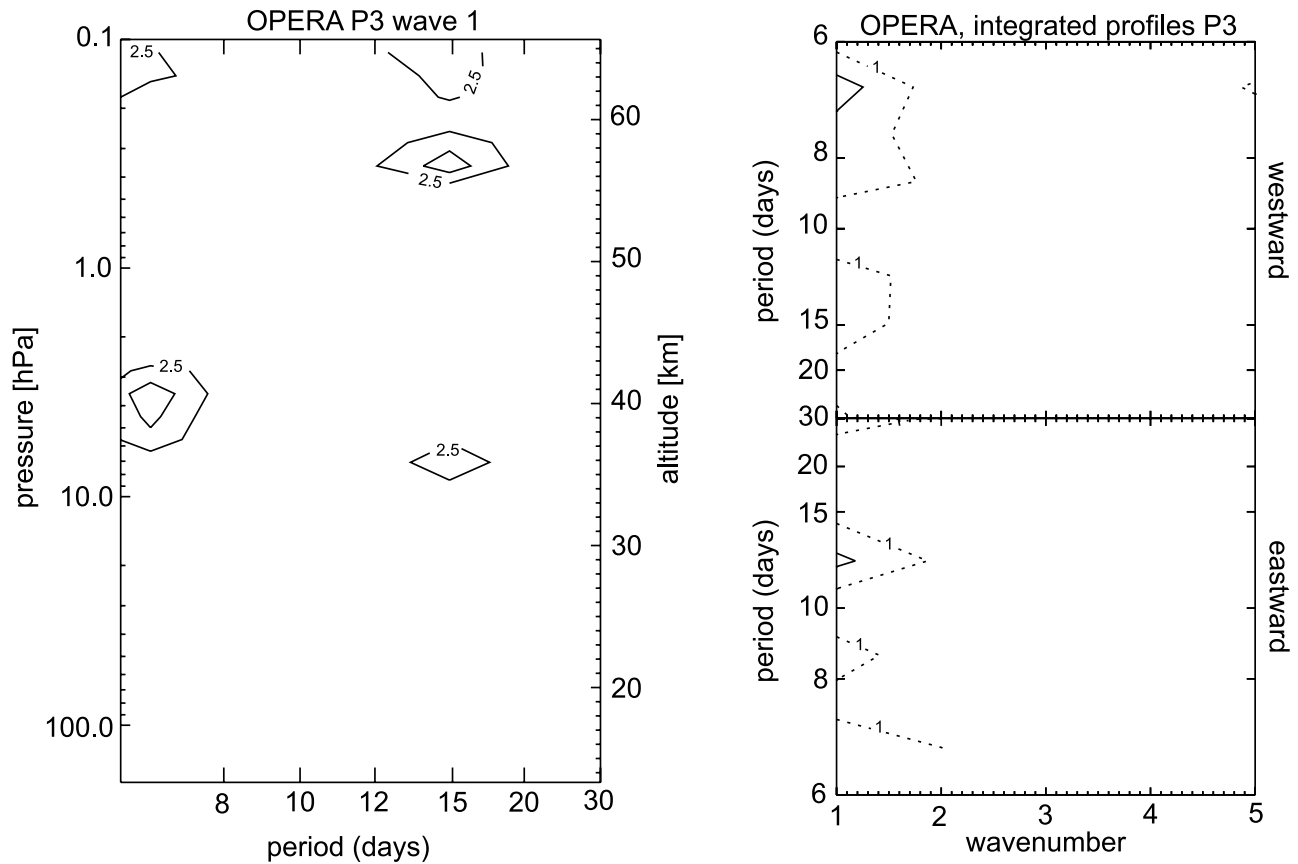
**Figure 3.** (left) Lomb periodogram for the OPERA ozone profiles, for zonal wave number 1 for the period 19 September to 18 November 2000. (right) Lomb periodogram for integrated OPERA ozone profiles for the period 19 September to 18 November 2000.

with

$$\tau_1 = \frac{1}{2\omega} atan \left[ \frac{\sum_j \sin 2\omega t_j}{\sum_j \cos 2\omega t_j} \right] \qquad (4)$$

$$\tau_2 = \frac{1}{2k} atan \left[ \frac{\sum_l \sin 2kx_l}{\sum_l \cos 2kx_l} \right] \qquad (5)$$

$$\bar{h} \equiv \frac{1}{N_{tot}} \sum_{j=1}^{N_t} \sum_{l=1}^{Nx} h(x_l, t_j) \qquad (6)$$

$$\sigma^2 \equiv \frac{1}{N_{tot} - 1} \sum_{j=1}^{N_t} \sum_{l=1}^{Nx} \left( h(x_l, t_j) - \bar{h} \right)^2 \qquad (7)$$

[23] The plus sign in equation (3) corresponds to westward traveling waves and the minus sign to eastward traveling waves.

[24] The periodogram values will give us an indication of the dominant frequencies in the data set.

[25] Before applying the periodogram, the OPERA and NNORSY O₃ profiles are regridded on a 5° × 5° grid by averaging over all measurements with center coordinates within the grid cell. Furthermore, 3-day averages of the OPERA and NNORSY profiles are taken since GOME

reaches global coverage in 3 days and 1 day averages would lead to numerous gaps in the data set. Please note that the 3-day averaging will affect the detection of fast Kelvin waves with periods shorter than 6 days (frequencies higher than the Nyquist frequency), these high frequencies will be falsely translated to frequencies lower than the Nyquist frequency. This study will thus focus on the slower Kelvin waves. The assimilated ozone profiles are provided daily with global coverage, so no time averaging has been applied. From all three data sets only the grid cells located at the equator are used in the analysis. We focus on this latitude band because Kelvin waves reach their maximum amplitude at the equator.

## 3. Results

[26] In this section we will show results for the three different data sets for periods with high Kelvin wave activity. Period P1 (15 July to 13 September 1996) and P3 (19 September to 18 November 2000) correspond to the first and third of the three periods with high Kelvin wave activity previously identified in the total ozone columns from GOME [*Timmermans et al.*, 2004]. The results for period P2 defined in the aforementioned paper are comparable to the results of period P1.

### 3.1. OPERA O₃ Profiles

[27] Figure 1 (left panel) shows the periodogram values for P1 as function of wave period and pressure for eastward
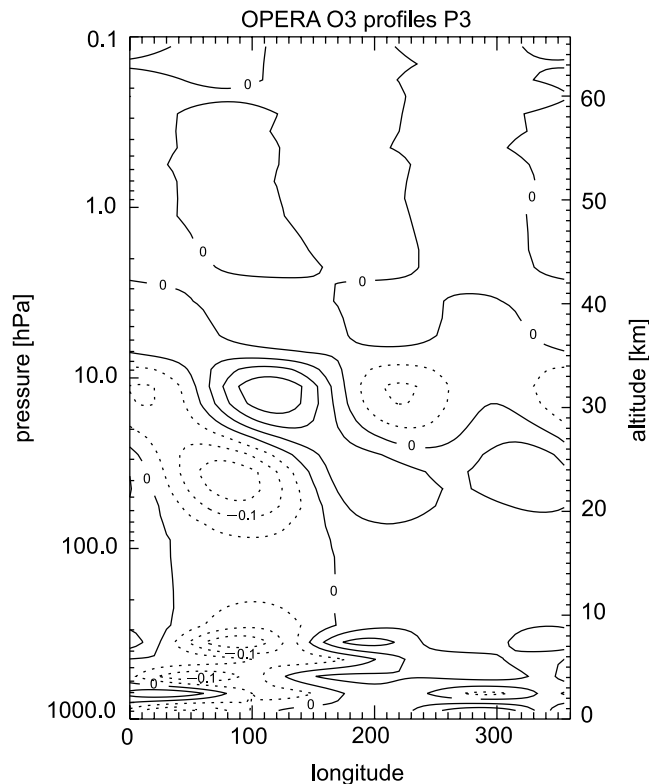
**Figure 4.** Pressure versus longitude plot of waves 1 and 2 in the OPERA ozone profiles on 27 October 2000. A band-pass filter with half-amplitudes at 12 and 20 days has been applied. Solid lines start at 0 DU/km with increments of 0.05 DU/km for each contour line. Dashed lines start at −0.05 DU/km with a decrement of 0.05 DU/km for each contour line. Here, 1 DU = $2.687 \times 10^{16}$ molecules/cm$^2$.

waves with zonal wave number 1 present in the OPERA ozone profile data. The maximum signal is found between about 10–50 hPa at wave periods of 15–20 days. This result agrees with the signal found in the GOME total ozone columns in T04. The right panel of Figure 1, which shows the periodogram of the integrated ozone profile as function of zonal wave number and wave period, agrees with the periodogram derived for the total ozone data (Figure 1, T04). The blue, green and red area respectively denote the 90%, 99% and 99,9% significant signals as explained in T04. Although somewhat less significant, which is expected since the integrated profile is less accurate than the dedicated ozone column, the signal in the integrated profile shows a very good agreement with the signal in the ozone columns.

[28] The left panel in Figure 2 shows a pressure versus longitude plot for the ozone perturbations on 23 August 1996 in P1, expected to be induced by Kelvin waves.

[29] To derive the perturbations that are expected to be induced by Kelvin waves, the data are filtered as to preserve only the dominant wave frequencies found in the periodogram. The filter only retains zonal wave numbers 1 and 2. In time a band-pass filter given by

*Murakami* [1979] is applied with half amplitudes at 12 and 20 days. 23 August 1996 is chosen because maximum ozone perturbations within period P1 are found on this day. Note that it is also the day where maximum zonal wind perturbations in the ERA-40 data were found in T05. From this figure of filtered data, the tilt of the perturbations with height can be determined. Between approximately 7 and 100 hPa a wave 1 structure is visible with an eastward phase tilt with height, characteristic for eastward moving Kelvin waves. However, the vertical extent of the positive and negative perturbations is too broad as can also be seen in the right panel of Figure 2. Here we took a cross section of the pressure longitude plot at a longitude of 85°, the location where we found our maximum ozone perturbations. The positive perturbations extent over the entire vertical range where we see the wave 1 structure and in the profile of the perturbations we see only one large maximum around 20 hPa and no clear vertical wave structure. It seems like the vertical resolution of the retrieved profiles is insufficient to resolve the vertical wave structure of the Kelvin waves.

[30] Although the vertical structure of the Kelvin waves is not completely resolved in our results for period P1, there is evidence of a Kelvin wave signal corresponding to the signal found in the GOME total ozone column data in T04. For period P3 this is not the case. While in the GOME ozone column data period P3 was identified as a period with high Kelvin activity, the OPERA ozone profiles do not show a clear Kelvin wave signal. Figure 3 (left panel) shows the periodogram values for P3 as function of wave period and pressure for eastward waves with zonal wave number 1 present in the OPERA ozone profile data. There is no maximum at the wave frequencies previously identified in the GOME ozone columns. The integrated ozone profile periodogram (Figure 3, right panel) does show a small signal at eastward propagating waves with wave number 1 and periods around 12 days, corresponding to the signal found in the GOME ozone columns. However, this signal is not significant. This is supported by looking at the pressure versus longitude plot for the ozone perturbations on 27 October 2000 in P3 (Figure 4), expected to be induced by waves with Kelvin wave characteristics. There is no eastward but a westward phase tilt with height, which is in contradiction with Kelvin wave theory. Further investigation of the data will be needed to examine what is causing these unexpected results.

## 3.2. NNORSY O₃ Profiles

[31] Figure 5 (left panel) shows the periodogram values for P1 as function of wave period and pressure for eastward waves with zonal wave number 1 present in the NNORSY ozone profile data. The maximum signal is found around 25 km at wave periods of 15 days in agreement with the signal found in the GOME total ozone columns in T04.

[32] The left panel in Figure 6 shows a pressure versus longitude plot for the ozone perturbations on 29 August 1996 in P1, expected to be induced by Kelvin waves. As with the OPERA profiles the data are filtered for zonal wave numbers 1 and 2 and in time a band-pass filter is
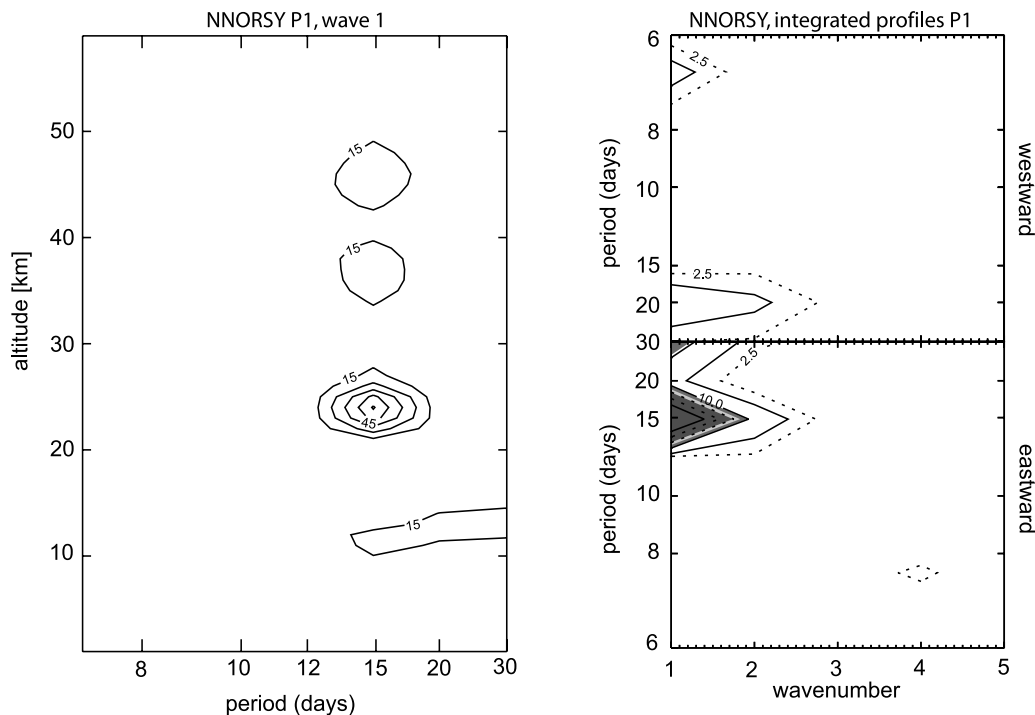
**Figure 5.** (left) Lomb periodogram for the NNORSY ozone profiles, for zonal wave number 1 for the period 15 July to 13 September 1996. (right) Lomb periodogram for integrated NNORSY ozone profiles for the period 15 July to 13 September 1996. See color version of this figure at back of this issue.
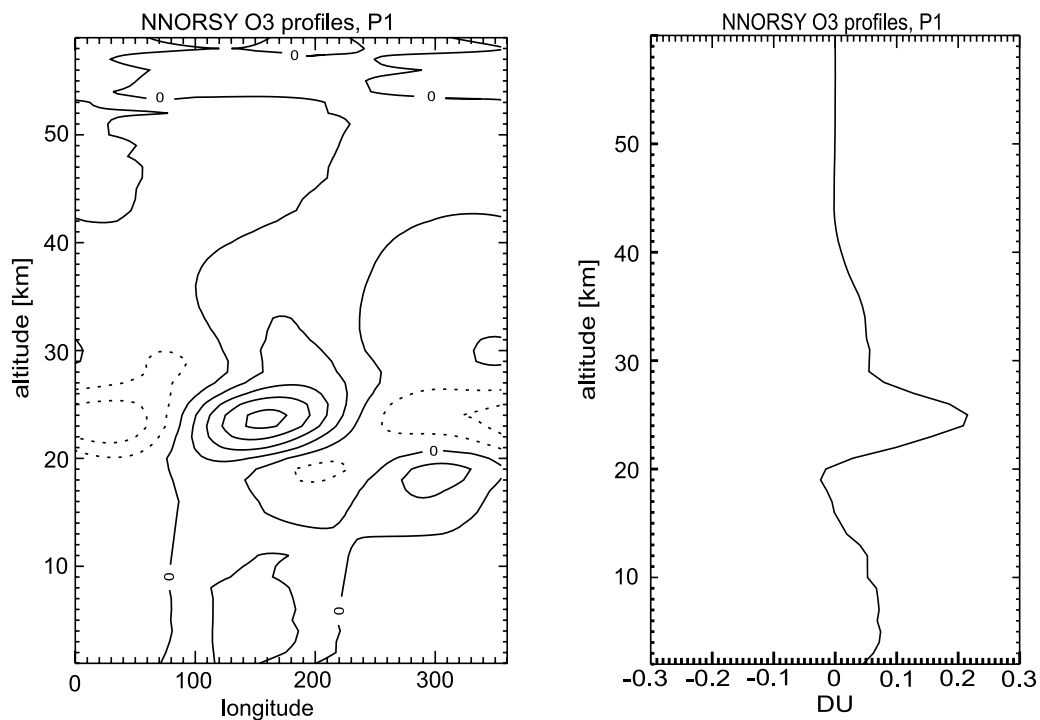


**Figure 6.** (left) Pressure versus longitude plot of waves 1 and 2 in the NNORSY ozone profiles on 29 August 1996. A band-pass filter with half-amplitudes at 12 and 20 days has been applied. Solid lines start at 0 DU/km with increments of 0.05 DU/km for each contour line. Dashed lines start at −0.05 DU/km with a decrement of 0.05 DU/km for each contour line. Here, 1 DU = 2.687 × 10$^{16}$ molecules/cm$^2$. (right) Profile of the ozone perturbations on 29 August 1996 at longitude equal to 160°.
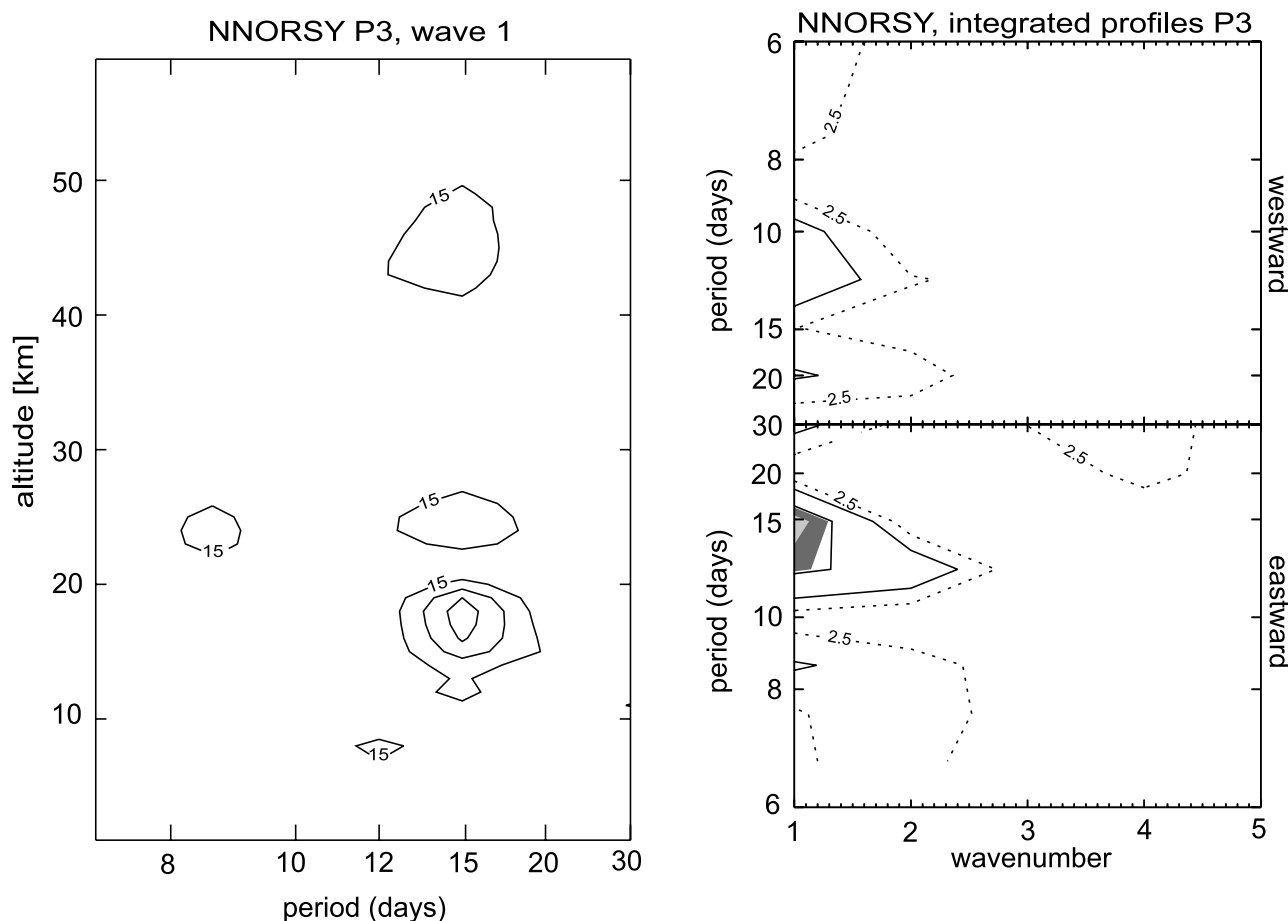
**Figure 7.** (left) Lomb periodogram for the NNORSY ozone profiles, for zonal wave number 1 for the period 19 September to 18 November 2000. (right) Lomb periodogram for integrated NNORSY ozone profiles for the period 19 September to 18 November 2000. See color version of this figure at back of this issue.

applied with half amplitudes at 12 and 20 days. 29 August 1996 is the date within period P1 where we find largest ozone perturbations in the NNORSY data. Between approximately 20 and 30 km a wave 1 structure is visible with an eastward phase tilt with height, characteristic for eastward moving Kelvin waves. Again the vertical extent of the positive and negative perturbations seems too broad. The right panel of Figure 6 shows a cross section of the pressure longitude plot at a longitude of 160°, the location where we found our maximum ozone perturbations. No vertical wave structure can be seen, there is one large maximum around 25 km. As with the OPERA profiles the vertical resolution of the retrieved profiles seems insufficient to fully resolve the vertical wave structure of the Kelvin waves.

[33] Similar to the results for the OPERA data set, the NNORSY data set also does not show a clear Kelvin wave signal in period P3. Figure 7 (left panel) shows the periodogram values for P3 as function of wave period and pressure for eastward waves with zonal wave number 1 present in the NNORSY ozone profile data. There is a maximum signal around 18 km and wave periods of 15 days, slightly larger than the wave periods of 12 days

where we found the maximum signal in the GOME ozone column. The integrated ozone profile periodogram (Figure 7, right panel) does show maximum signal at eastward propagating waves with wave number 1 and periods around 12–15 days. However, when looking at the pressure versus longitude plot for the ozone perturbations on 30 September 2000 in P3 (Figure 8), we do not see the eastward phase tilt with height that is characteristic for Kelvin waves.

### 3.3. Assimilated OPERA O₃ Profiles

[34] Figure 9 shows the periodogram values for P1 and P3 as function of wave period and pressure for eastward waves with zonal wave number 1 present in the assimilated OPERA ozone profile data. For P1 maxima can be seen around 5 and 40 hPa at wave periods of 15–20 days in agreement with the signal found in the GOME total ozone columns in T04. Another maximum for P1 is seen around 10 hPa at wave periods of 30 days. Because we calculate the periodogram values over 60-day periods, waves with periods of 30 days are the slowest waves we can detect; therefore the reliability of the detection close to 30 days

## NNORSY O3 profiles, P3
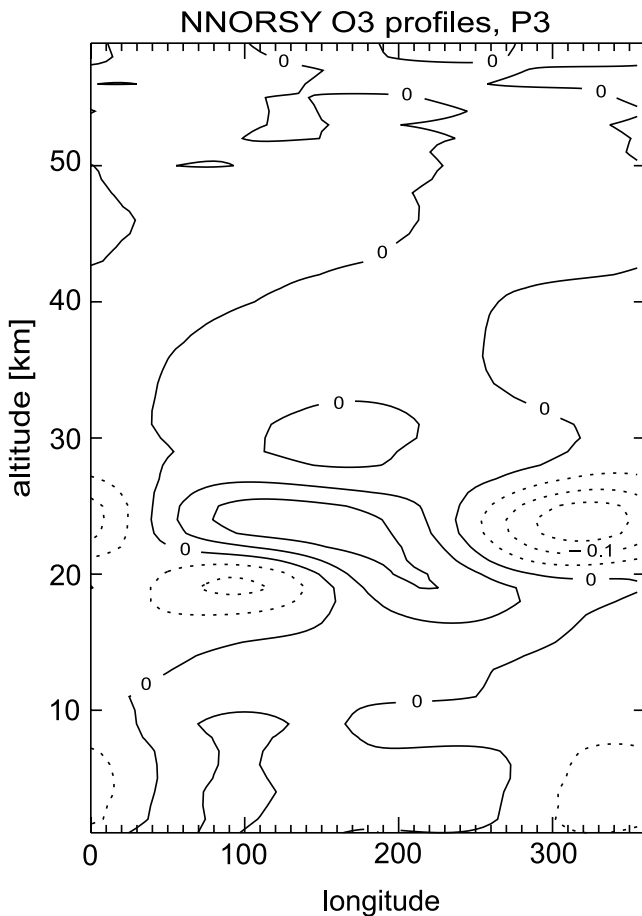


**Figure 8.** Pressure versus longitude plot of waves 1 and 2 in the NNORSY ozone profiles on 30 September 2000. A band-pass filter with half-amplitudes at 12 and 20 days has been applied. Solid lines start at 0 DU/km with increments of 0.05 DU/km for each contour line. Dashed lines start at −0.05 DU/km with a decrement of 0.05 DU/km for each contour line. Here, 1 DU = 2.687 × 10¹⁶ molecules/cm².

is doubtful. For P3, maxima can be seen around 7 hPa and 30–40 hPa at wave periods of 15 days.

[35] Figure 10 shows pressure versus longitude plots for the ozone perturbations on 13 August 1996 in P1 and 23 October 2000 in P3, expected to be induced by Kelvin waves. The same filters have been applied as with the previous two data sets. In this data set 13 August 1996 and 23 October 2000 are the dates within the periods P1 and P3 where we find largest ozone perturbations in DU/km. In contrast with the results from the two previous data sets, here in both P1 and P3 a wave 1 structure is visible with the eastward phase tilt with height, characteristic for Kelvin waves. This structure is visible between ~20 and 70 hPa for P1 and between ~10 and 70 hPa for P3.

[36] In Figure 11, cross sections of the pressure longitude plots at a longitude of 129° for P1 and 297° for P3, are shown. These are the locations where we found our maximum ozone perturbations. Maximum (negative) amplitudes of 0.65 DU/km and 0.42 DU/km are seen

around 30–40 hPa, where the gradient in ozone is largest. These results are in agreement with previous studies [e.g., *Kawamoto et al.*, 1997; *Mote and Dunkerton*, 2004]. Integrating the profiles of the ozone perturbations lead to maximum total ozone column perturbations of 1.2 DU in P1 and 1.9 DU in P3. These results compare well with the fluctuations found in the GOME total ozone columns of 1–2 DU.

[37] In Figure 12 the same cross sections as in Figure 11 are shown but now the ozone fluctuations derived from the ERA-40 temperature fluctuations are shown. The calculation, which is explained in T05, is based on linear Kelvin wave theory and only includes transport effects. Photochemical effects on ozone are neglected. Ozone perturbations are then given by [*Salby et al.*, 1990, equation (9)]

$$\chi' = \frac{\frac{\partial \bar{\chi}}{\partial z}}{S} T' \qquad (8)$$

where $S = HN^2/R$ is a background static stability parameter. Thus, when only considering transport effects, the induced ozone fluctuations are proportional to the vertical gradient in mean ozone and in phase with the temperature fluctuations for a positive vertical gradient of ozone. The altitude of the calculated maxima agrees very well with the altitude of the maxima in the assimilated OPERA data. The agreement between the maximum amplitude around 35 hPa of the calculated ozone fluctuations and the maximum amplitude of the ozone fluctuations in the assimilated OPERA is very good for period P3. For period P1, the maximum in calculated ozone fluctuations is slightly smaller than the maximum amplitude for the assimilated OPERA ozone. There are several possible reasons for this discrepancy, e.g., the vertical gradient in the ozone profile is larger than the values used in the calculation, the ozone fluctuations are not only caused by transport effects but also by photochemical effects, the temperature perturbations in the ERA-40 data are too small or the ozone fluctuations in the assimilated OPERA data are too large.

[38] A striking difference between the results for the assimilated and simulated profile is the damping of structures below 80 hPa for the assimilated profiles, similar to the results for the retrieved profiles. Apparently, the vertical resolution of the assimilated profiles below 80 hPa is not much better than for the retrieved profiles. This is contrary to our conclusion in section 2.4 that the resolution would be improved by the inclusion of model (transport) information. *Segers et al.* [2004] note that the assimilated profiles in the tropical troposphere show relatively large biases. We conclude that the quality of this data set is at present inadequate in the tropical troposphere to draw conclusions on the (Kelvin wave) variability in ozone.

[39] Figure 13 shows the time evolution of the normalized ERA-40 temperature perturbations in combination with the normalized assimilated OPERA ozone mixing ratio perturbations at the altitude where we found maximum ozone perturbations. The two variables are nearly in phase for the 60-day period P1. However, on 13 August 1996 where maximum ozone perturbations are seen, the
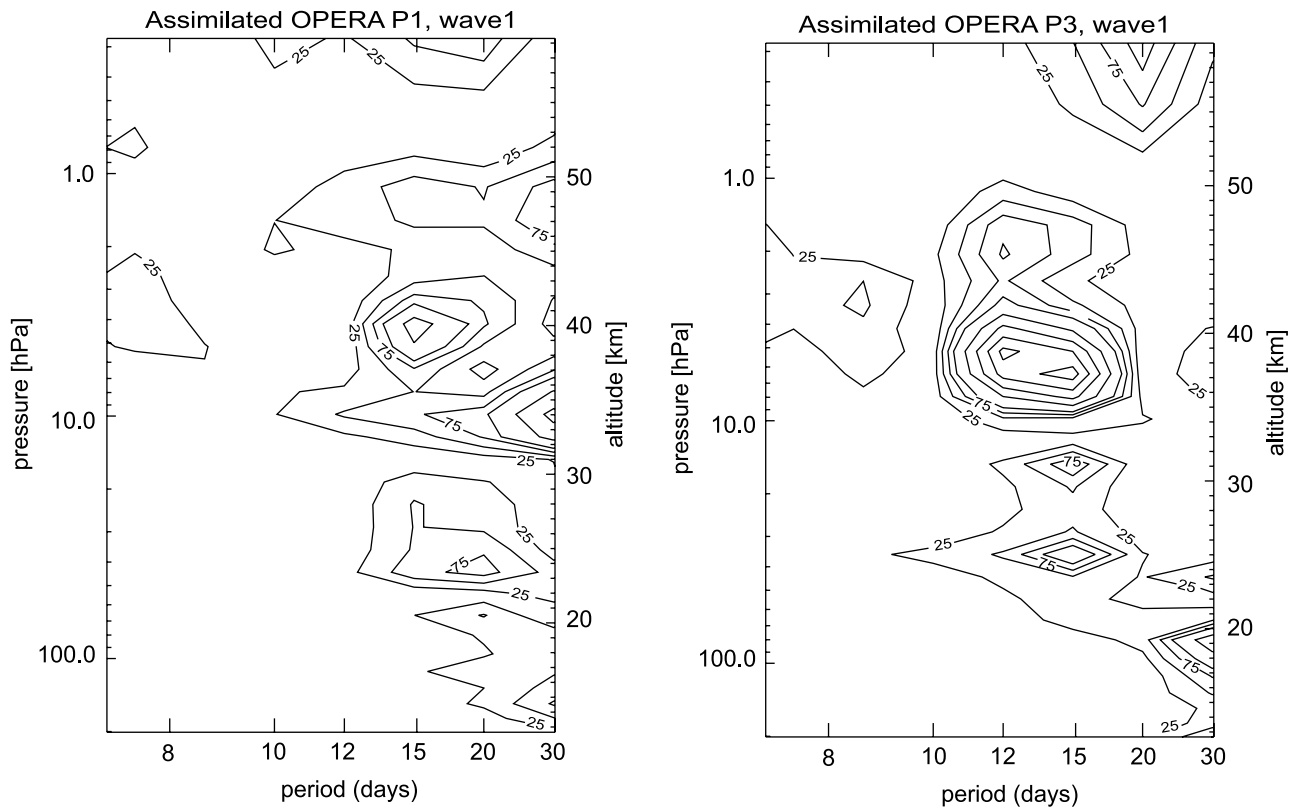
**Figure 9.** Lomb periodogram for the assimilated OPERA ozone profiles, for zonal wave number 1 for the periods (left) 15 July to 13 September 1996 and (right) 19 September to 18 November 2000.

temperature perturbations are not at their maximum yet. This might explain the discrepancy between the calculated ozone perturbations and the perturbations in the assimilated OPERA ozone. In contrast, on 23 October 2000 the ozone and temperature perturbations are in phase, supporting the good agreement between the maximum amplitudes on this date.

[40] Figures 14 and 15 show pressure versus time plots of the ozone perturbations in P1 and P3, both in DU/km and ppmv. Large perturbations in the mixing ratio of ozone (ppmv) above 10 hPa can be seen that especially in P3 are out of phase with the perturbations below 10 hPa. This may be caused by the change in sign of the vertical ozone gradient or increasing photochemical effects [*Mote and Dunkerton*, 2004; *Salby et al.*, 1990]. The perturbations above 10 hPa disappear when converting to DU and hence will not make a large contribution to the total ozone column perturbations.

[41] As can be seen in Figure 16 these large ozone perturbations above 10 hPa are out of phase with ERA-40 temperature perturbations. Since the vertical gradient of ozone is negative at these altitudes, the ozone perturbations can be caused by transport effects following equation (8). At these altitudes however, photochemical influences on ozone can also start playing a role. Following *Salby et al.* [1990], ozone fluctuations will be photochemically controlled at altitudes above 4 hPa and consequently show an out-of-phase relationship with temperature perturbations. Further investigation including

information on the photochemical effect on the ozone perturbations will be needed to determine the source of the ozone perturbations above 10 hPa.

## 4. Conclusion and Discussion

[42] Three different sets of GOME ozone profile data have been studied to investigate the ability of retrieving information on Kelvin wave activity and its horizontal and vertical structure.

[43] Two of the data sets (OPERA and NNORSY) do provide some information on Kelvin wave activity but cannot fully resolve the vertical structure of the Kelvin waves. They do, however, show that the Kelvin waves have their largest amplitudes between 20 and 30 km in agreement with theory. In these two data sets Kelvin wave signals are present, in some cases weak, in agreement with signals previously identified in the GOME total ozone columns.

[44] The third data set, which consists of assimilated OPERA ozone profiles, is able to provide more height-resolved information on the structure of identified Kelvin wave activity. Since the OPERA profiles do not contain this information, it must be originating from the ECMWF meteorological fields that are driving the assimilation model. The assimilated ozone profiles show variability that is in agreement with results previously found in the GOME ozone columns and ERA-40 temperature and zonal wind fields. The variability corresponds to eastward propagating waves with zonal wave numbers 1 and 2 and wave periods
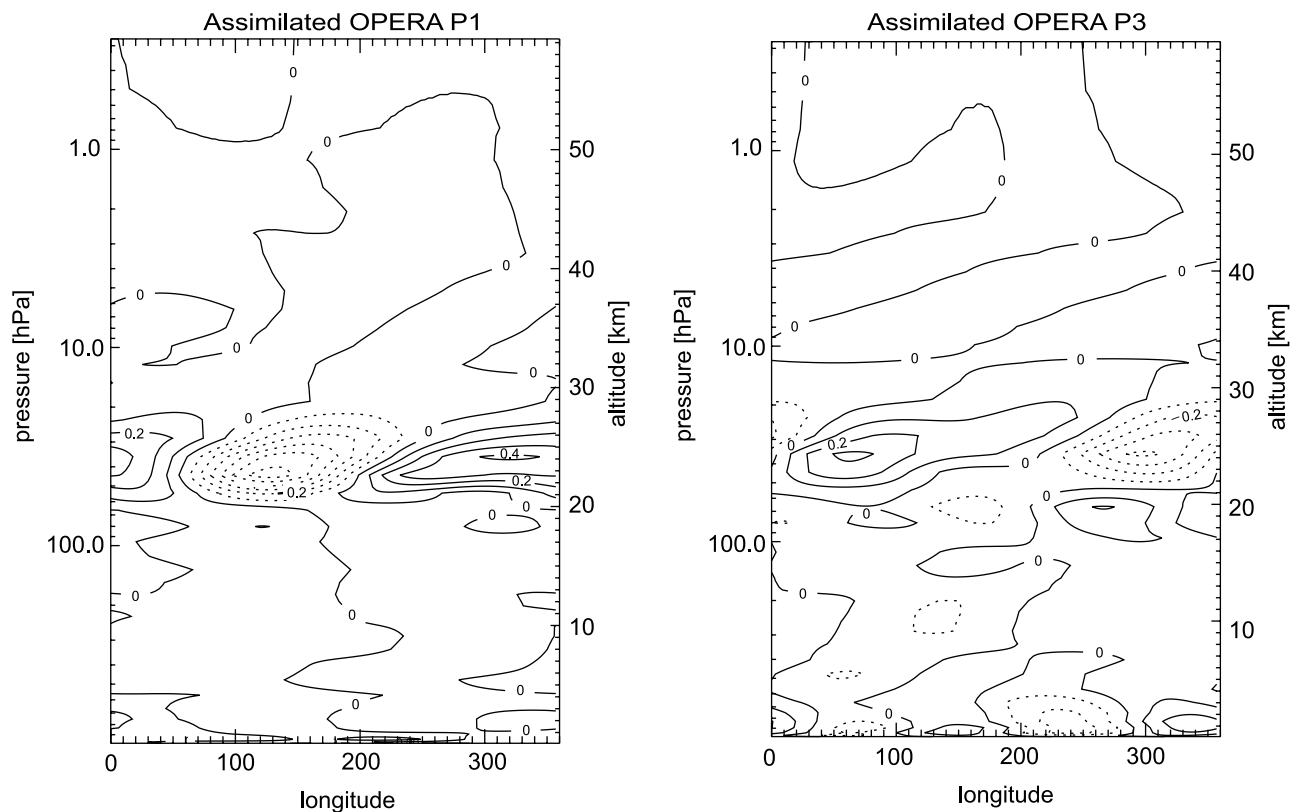
**Figure 10.** Pressure versus longitude plot of waves 1 and 2 in the assimilated OPERA ozone profiles on (left) 13 August 1996 and (right) 23 October 2000. A band-pass filter with half-amplitudes at 12 and 20 days has been applied. Solid lines start at 0 DU/km with increments of 0.1 DU/km for each contour line. Dashed lines start at −0.1 DU/km with a decrement of 0.1 DU/km for each contour line. Here, 1 DU = 2.687 × 10$^{16}$ molecules/cm$^2$.
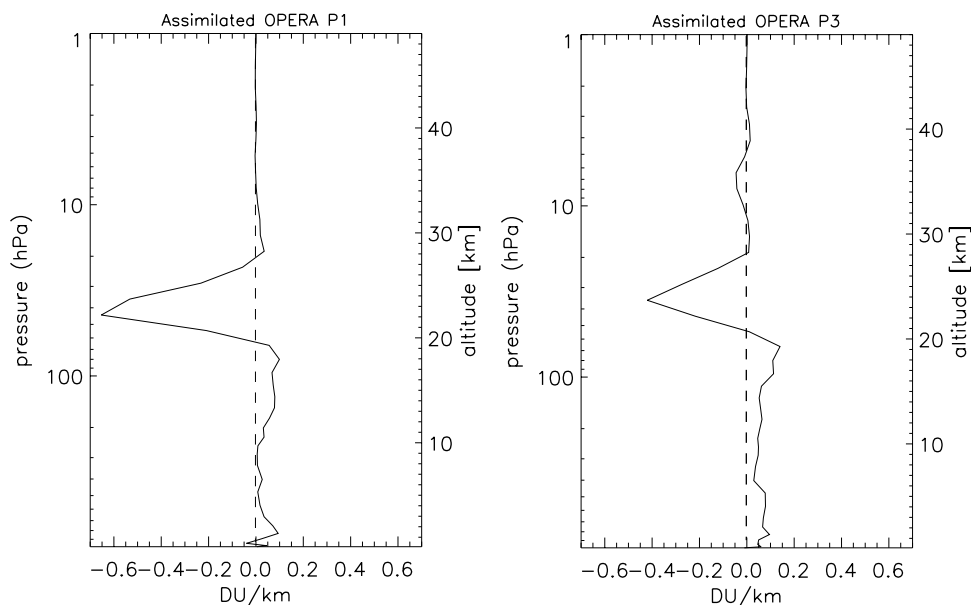
**Figure 11.** Profiles of the ozone perturbations in the assimilated OPERA ozone profiles on (left) 13 August 1996 at longitude equal to 129° and (right) 23 October 2000 at longitude equal to 297°. Here, 1 DU = 2.687 × 10$^{16}$ molecules/cm$^2$.
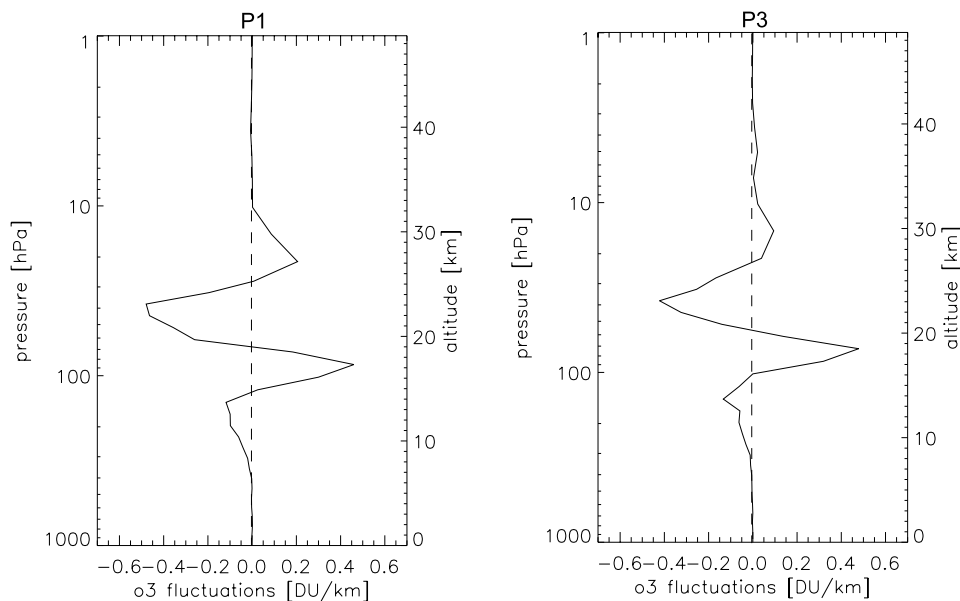
**Figure 12.** Profiles of the ozone perturbations derived from the ERA-40 temperature perturbations on (left) 13 August 1996 at longitude equal to 130° and (right) 23 October 2000 at longitude equal to 295°. Here, 1 DU = 2.687 × 10¹⁶ molecules/cm².

between 12 and 20 days. The Kelvin-wave-induced ozone perturbations have amplitudes of up to 0.65 DU/km or 0.2 ppmv. Integrating these perturbations in the vertical give maximum total ozone columns perturbations of 1.2 to 1.9 DU, depending on the chosen period. These values are consistent with the maximum perturbations of 1–2 DU previously found in the GOME total ozone columns. The maximum ozone perturbations are found at the altitude where the vertical gradient in ozone is largest, around 35 hPa. At this altitude the ozone perturbations are nearly in phase with ERA-40 temperature perturbations, supporting the suggestion that these ozone perturbations in the lower stratosphere are induced by transport effects. The agreement between the ozone perturbations in the assimilated OPERA data and calculated ozone perturbations that are derived from the ERA-40 temperature perturbations, considering transport effects only, is good concerning the altitude and amplitude of maximum perturbations. In the tropical troposphere the calculated ozone perturbations show large perturbations that are not resolved by the assimilated data, possibly because of previously reported problems with this data set in the troposphere.

[45] Between 10 and 1 hPa large fluctuations in the ozone mixing ratio are present that diminish in the conversion to DU. These higher-altitude perturbations are out of phase with the ERA-40 temperature perturbations. Since the vertical gradient in ozone changes sign above 10 hPa, these perturbations could be induced by transport effects. However, at these altitudes photochemical influences on ozone can also start paying a role. Further investigation will be needed to be able to determine the source of the ozone perturbations above 10 hPa.

[46] To be able to resolve fine vertical structure in ozone profiles, an adequate vertical resolution of the measurements is needed. The Scanning Imaging Absorption Spectrometer for Atmospheric Chartography (SCIAMACHY)
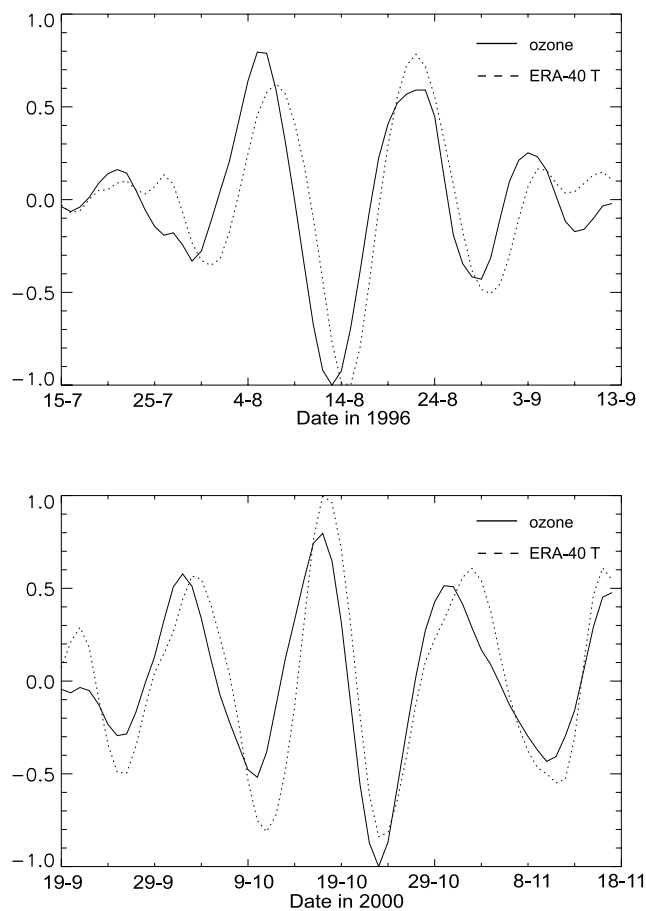


**Figure 13.** Normalized ERA-40 temperature (dashed lines) and assimilated OPERA ozone (solid lines) mixing ratio (ppmv) perturbations. (top) For period P1 at 44 hPa and longitude equal to 130° for temperature and 129° for ozone. (bottom) For period P3 at 36 hPa and longitude equal to 295° for temperature and 297° for ozone.
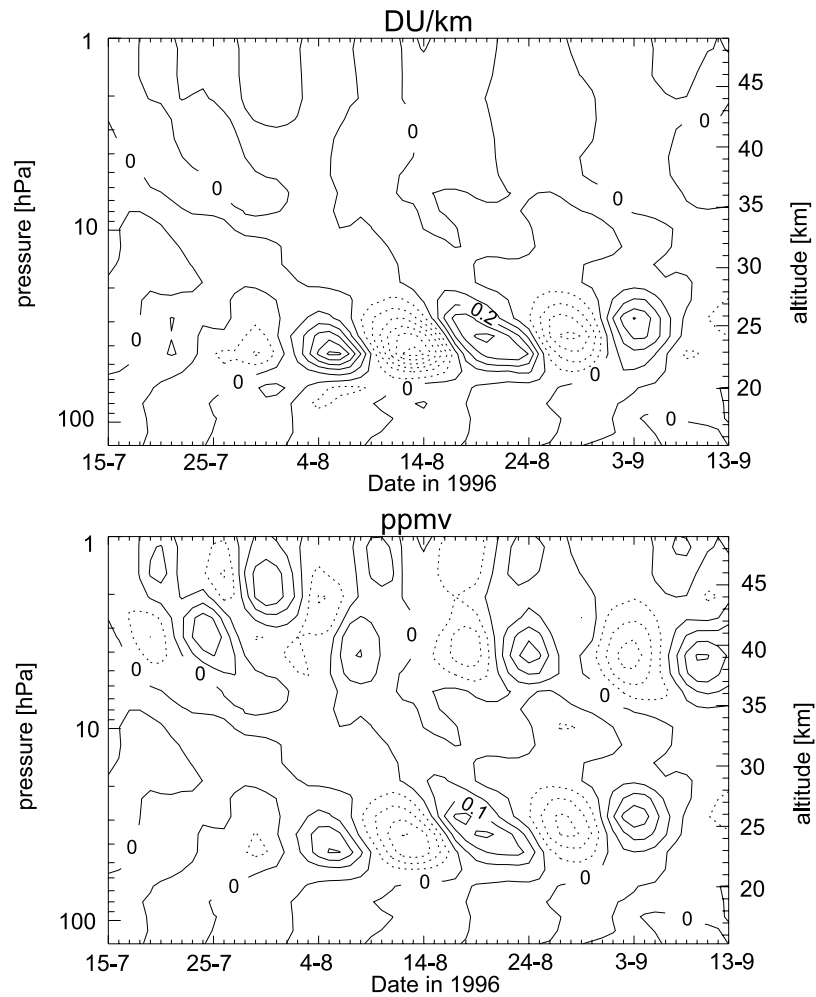
**Figure 14.** Pressure versus time plots of the ozone perturbations for period P1 and longitude equal to 129° in (top) DU/km and (bottom) ppmv. Solid contour lines start at 0 DU/km and 0 ppmv with increments of 0.1 DU/km and 0.05 ppmv for each contour line. Dashed lines start at −0.1 DU/km and −0.05 ppmv with a decrement of 0.1 DU/km and 0.05 ppmv for each contour line. 1 DU = 2.687 × 10¹⁶ molecules/cm².
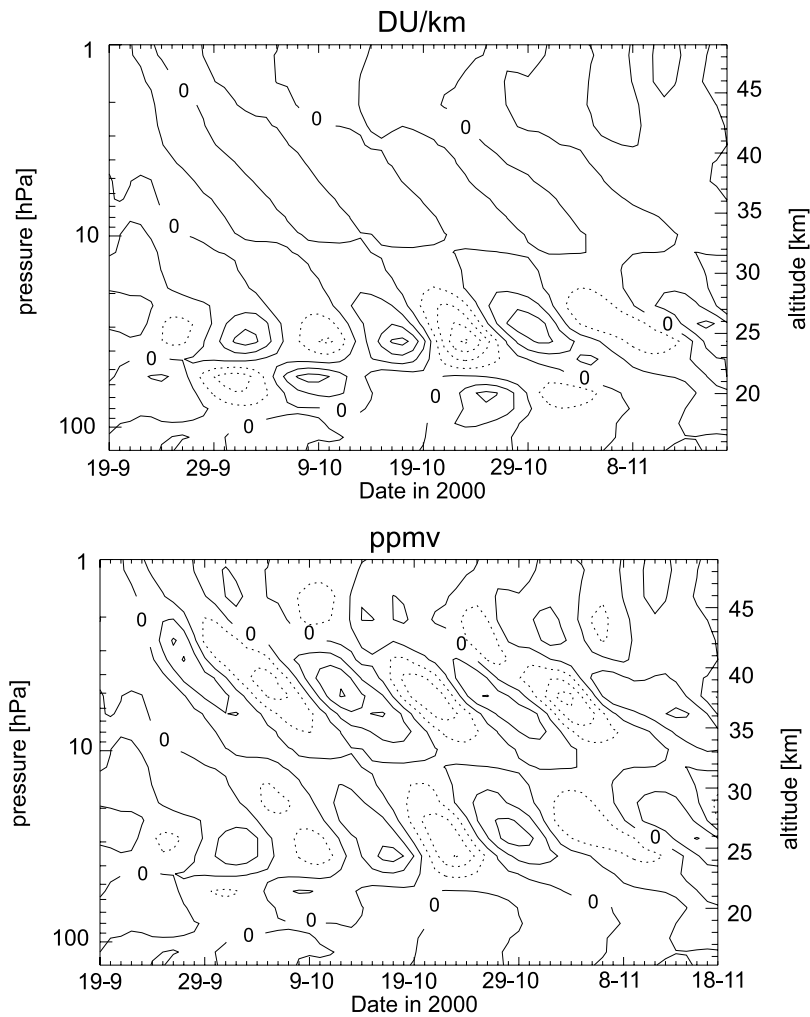
**Figure 15.** Pressure versus time plots of the ozone perturbations for period P3 and longitude equal to 297° in (top) DU/km and (bottom) ppmv. Solid contour lines start at 0 DU/km and 0 ppmv with increments of 0.1 DU/km and 0.05 ppmv for each contour line. Dashed lines start at −0.1 DU/km and −0.05 ppmv with a decrement of 0.1 DU/km and 0.05 ppmv for each contour line. Here, 1 DU = 2.687 × 10$^{16}$ molecules/cm$^2$.
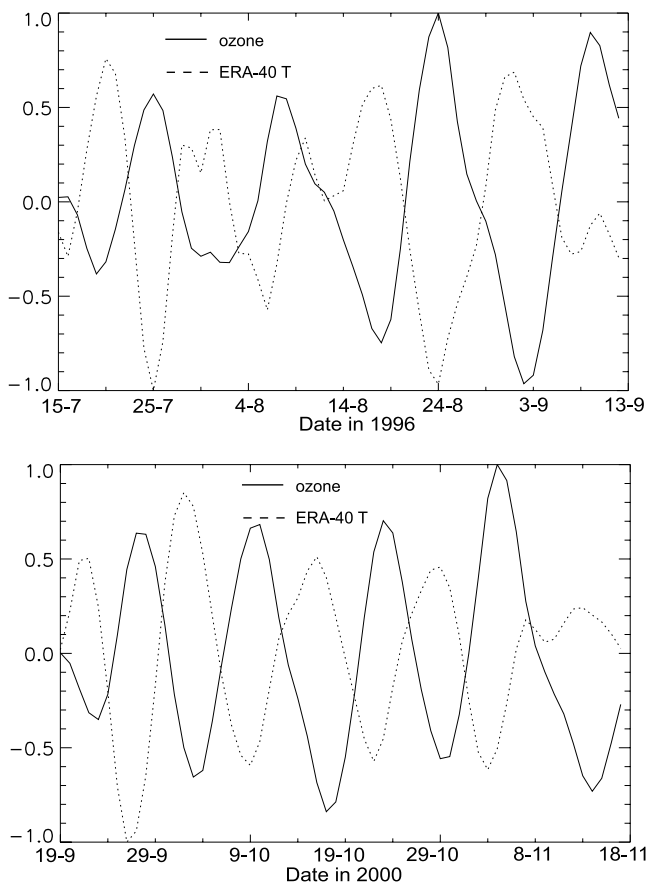
**Figure 16.** Normalized ERA-40 temperature (dashed lines) and assimilated OPERA ozone (solid lines) mixing ratio (ppmv) perturbations. (top) For period P1 at 4.2 hPa and longitude equal to 125° for temperature and 123° for ozone. (bottom) For period P3 at 5.2 hPa and longitude equal to 215° for temperature and 216° for ozone.

instrument on board Environmental Satellite (Envisat), performs limb measurements of ozone with a vertical resolution of ~3 km. In future, the combination of these measurements with the nadir measurements of the instrument providing total ozone columns is expected to form a unique mean for investigating both horizontal and vertical structure of the Kelvin wave activity.

## References

Andrews, D. G., J. R. Holton, and C. B. Leovy (1987), *Middle Atmosphere Dynamics*, Elsevier, New York.
Boehm, M. T., and J. Verlinde (2000), Stratospheric influence on upper tropospheric tropical cirrus, *Geophys. Res. Lett.*, 27, 3209–3212.
Burrows, J. P., et al. (1999), The Global Ozone Monitoring Experiment (GOME): Mission concept and first scientific results, *J. Atmos. Sci.*, 56, 151–175.
Canziani, P. O. (1999), Slow and ultraslow equatorial Kelvin waves: The UARS-CLAES view, *Q. J. R. Meteorol. Soc.*, 125, 657–676.
Cariolle, D., and M. Déqué (1986), Southern Hemisphere medium-scale waves and total ozone disturbances in a spectral general circulation model, *J. Geophys. Res.*, 91, 10,825–10,846.

Fortuin, J. P. F., and H. M. Kelder (1998), An ozone climatology based on ozonesondes and satellite measurements, *J. Geophys. Res.*, 103, 31,709–31,734.
Hadjinicolaou, P., and J. A. Pyle (2004), The impact of arctic ozone depletion on northern middle latitudes: Interannual variability and dynamical control, *J. Atmos. Chem.*, 47(1), 25–43.
Hirota, I. (1978), Equatorial waves in the upper stratosphere and mesosphere in relation to the semiannual oscillation of the zonal wind, *J. Atmos. Sci.*, 35, 714–722.
Holton, J. R., M. J. Alexander, and M. T. Boehm (2001), Evidence for short vertical wavelength Kelvin waves in the Department of Energy-Atmospheric Radiation Measurement Nauru99 radiosonde data, *J. Geophys. Res.*, 106, 20,125–20,129.
Kawamoto, N., M. Shiotani, and J. C. Gille (1997), Equatorial Kelvin waves and corresponding tracer oscillations in the lower stratosphere as seen in LIMS data, *J. Meteorol. Soc. Japan*, 75, 763–773.
McLinden, C. A., S. C. Olsen, B. Hannegan, O. Wild, M. J. Prather, and J. Sundet (2000), Stratospheric ozone in 3-D models: A simple chemistry and the cross-tropopause flux, *J. Geophys. Res.*, 105(D11), 14,653–14,665.
Meijer, Y. J., R. J. van der A, R. F. van Oss, D. P. J. Swart, H. M. Kelder, and P. V. Johnston (2003), Global Ozone Monitoring Experiment ozone profile characterization using interpretation tools and lidar measurements for intercomparison, *J. Geophys. Res.*, 108(D23), 4723, doi:10.1029/2003JD003498.
Mote, P. W., and T. J. Dunkerton (2004), Kelvin wave signatures in stratospheric trace constituents, *J. Geophys. Res.*, 109, D03101, doi:10.1029/2002JD003370.
Müller, M. D., A. K. Kaifel, M. Weber, S. Tellmann, J. P. Burrows, and D. Loyola (2003), Ozone profile retrieval from Global Ozone Monitoring Experiment (GOME) data using a neural network approach (Neural Network Ozone Retrieval System (NNORSY)), *J. Geophys. Res.*, 108(D16), 4497, doi:10.1029/2002JD002784.
Murakami, M. (1979), Large scale aspects of deep convective activity over the GATE area, *Mon. Weather Rev.*, 107, 994–1013.
Press, W. H., S. A. Teukolsky, W. T. Vetterling, and B. P. Flannery (1992), *Numerical Recipes in Fortran (or in C or in Pascal): The Art of Scientific Computing*, 2nd ed., Cambridge Univ. Press, New York.
Randel, W. J., and J. C. Gille (1991), Kelvin wave variability in the upper stratosphere observed in SBUV ozone data, *J. Atmos. Sci.*, 48, 2336–2349.
Salby, M. L., P. Callaghan, S. Solomon, and R. Garcia (1990), Chemical fluctuations associated with vertically propagating equatorial Kelvin waves, *J. Geophys. Res.*, 95, 20,491–20,505.
Scargle, J. D. (1982), Studies in astronomical time series analysis II. Statistical aspects of spectral analysis of unevenly spaced data, *Astrophys. J.*, 263, 835–853.
Segers, A. J., H. J. Eskes, R. J. van der A, R. F. van Oss, and P. F. J. Velthoven (2004), Assimilation of GOME ozone profiles and a global chemistry-transport model, *Q. J. R. Meteorol. Soc.*, 130, 477–502.
Smith, A. K., P. Preusse, and J. Oberheide (2002), Middle atmosphere Kelvin waves observed in Cryogenic Infrared Spectrometers and Telescopes for the Atmosphere (CRISTA) 1 and 2 temperature and trace species, *J. Geophys. Res.*, 107(D23), 8177, doi:10.1029/2001JD000577.
Timmermans, R. M. A., R. F. van Oss, and H. M. Kelder (2004), Equatorial Kelvin wave signatures in ozone column measurements from GOME, *J. Geophys. Res.*, 109(D1), D01101, doi:10.1029/2003JD003946.
Timmermans, R. M. A., R. F. van Oss, and H. M. Kelder (2005), Kelvin wave signatures in ECMWF meteo fields and GOME ozone columns, *J. Geophys. Res.*, 110, D13104, doi:10.1029/2004JD005261.
van der A, R. J., R. F. van Oss, A. J. M. Piters, J. P. F. Fortuin, Y. J. Meijer, and H. M. Kelder (2002), Ozone profile retrieval from recalibrated Global Ozone Monitoring Experiment data, *J. Geophys. Res.*, 107(D15), 4239, doi:10.1029/2001JD000696.
van Oss, R. F., and R. J. D. Spurr (2002), Fast and accurate 4 and 6 stream linearised discrete ordinate radiative transfer models for ozone profile remote sensing retrieval, *J. Quant. Spectrosc. Radiat. Transfer*, 75, 177–220.
Wallace, J. M., and V. E. Kousky (1968), Observational evidence of Kelvin waves in the tropical stratosphere, *J. Atmos. Sci.*, 25, 900–907.
Ziemke, J. R., and J. L. Stanford (1994), Kelvin waves in total column ozone, *Geophys. Res. Lett.*, 21, 105–108.

H. M. Kelder and R. F. van Oss, Royal Netherlands Meteorological Institute, P. O. Box 201, NL-3730 AE De Bilt, Netherlands.
R. M. A. Timmermans, Environment, Health, and Safety, Netherlands Organisation for Applied Scientific Research TNO, NL-7300 AH Apeldoorn, Netherlands. (timmermans@mep.tno.nl)
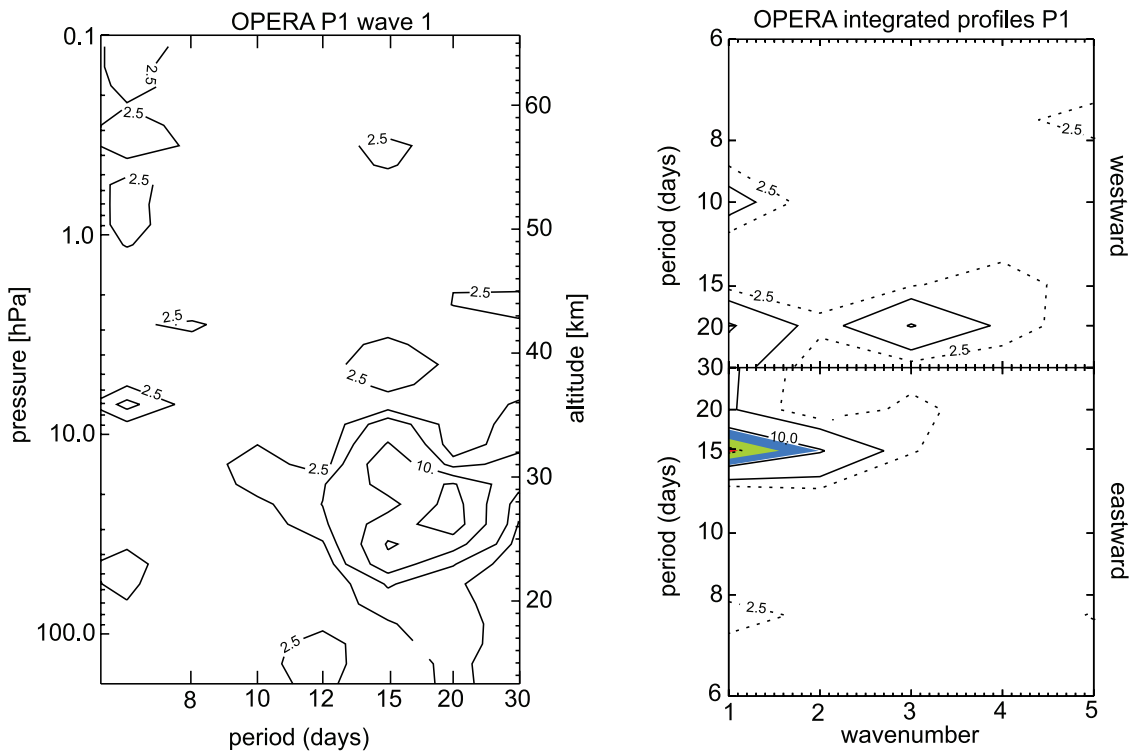
**Figure 1.** (left) Lomb periodogram for the OPERA ozone profiles, for zonal wave number 1 for the period 15 July to 13 September 1996. (right) Lomb periodogram for integrated OPERA ozone profiles for the period 15 July to 13 September 1996.
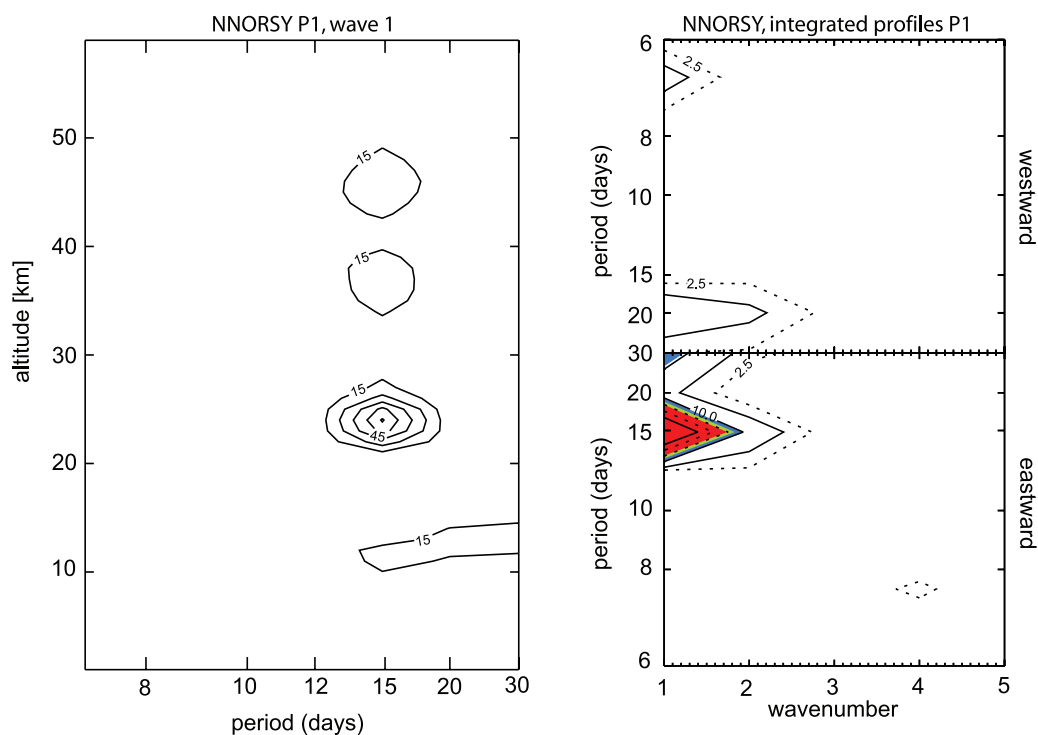


**Figure 5.** (left) Lomb periodogram for the NNORSY ozone profiles, for zonal wave number 1 for the period 15 July to 13 September 1996. (right) Lomb periodogram for integrated NNORSY ozone profiles for the period 15 July to 13 September 1996.

**Figure 7.** (left) Lomb periodogram for the NNORSY ozone profiles, for zonal wave number 1 for the period 19 September to 18 November 2000. (right) Lomb periodogram for integrated NNORSY ozone profiles for the period 19 September to 18 November 2000.